

# **HiSST: 4th International Conference on High-Speed Vehicle Science Technology**

22 -26 September 2025, Tours, France



# Design of the Landing Stability Test for the ESA Space Rider Project

A.C. Esposito<sup>1</sup>, R. Gardi<sup>1</sup>, A. De Fenza<sup>1</sup>, P. Vernillo<sup>1</sup>, V. Paolella<sup>1</sup>, I. Di Criscio<sup>1</sup>, G. Rufolo<sup>1</sup>

#### Abstract

This paper presents the design of the Landing Stability Test (LST) for the Space Rider Project, a reusable uncrewed orbital platform developed by the European Space Agency (ESA) under the primership of Thales Alenia Space Italia and AVIO. The LST aims to evaluate the dynamic response and structural integrity of the Re-Entry Module under controlled landing scenarios, ensuring that sensitive scientific payloads are protected from excessive shocks. The paper describes the methodology used to design a representative mock-up of the Space Rider Re-entry Module, in terms of mass and inertia, and a dedicated test facility capable of achieving the required velocities and attitudes at ground impact. The activity is developed in the frame of the system level verification activities of the descent and landing phase in charge to the Italian Aerospace Research Center as subcontractor of Thales Alenia Space Italia.

**Keywords**: Ground Facility Testing, Landing Gear, Structure & Mechanisms

#### Nomenclature

CAD - Computer-Aided Design

CoG – Center of Gravity

FEM - Finite Element Method

IA - Interface Assembly

IP – In-Plane

J – Objective function

LA - Landing Assembly

LG - Landing Gear

LTM – Landing Test Model

LTR - Landing Test Rig

LST – Landing Stability Test

MCI - Mass, Center of gravity, Inertia

OOP - Out-Of-Plane

P – Penalty function

R – Position vector

RM - Re-entry Module

W - Weight

a, b - Base dimensions of ballasts

h – Heiaht

m – Mass

r – Input vector

x, y, z - Cartesian coordinates

Greek

a – weighting coefficient

 $\delta$  – Deviation

ρ – Density

Subscripts

A, B, C – Load cell labels

Reg – Required value from specifications

#### 1. Introduction

The ESA Space Rider project is based on the development of a reusable spacecraft designed for missions in Low Earth Orbit (LEO). The re-entry and landing phases are among the most critical aspects of the mission, as they ensure a safe and stable return of the spacecraft and satisfy the reusability requirement. As part of the design and validation process, a complex helicopter drop test has been devised to evaluate the subsonic phase of the flight and the landing. In this context, the LST is intended to demonstrate that the Landing Sub-system can ensure a stable landing of the Space Rider Re-entry Module (RM) upon impact with the prepared landing terrain. This objective is achieved through a dedicated facility composed of two main components: a mock-up of the Re-entry Module, called the Landing Test Model (LTM), and a dedicated Landing Test Rig (LTR), which accelerates the LTM to

<sup>&</sup>lt;sup>1</sup> CIRA, via Maiorise 81043 Capua CE, a.esposito@cira.it

reproduce the conditions required for the various test configurations.

The following paragraphs describe the design requirements, followed by a detailed presentation of the LTM and LTR. Particular attention is given to achieving the Mass, Center of gravity, and Inertia (MCI) requirements of the LTM, using an iterative approach based on a multi-variable optimization code. FEM analyses are also included and presented to verify the modal response and mechanical strength of the test article.

# 2. Requirements

The LST is designed to cover various landing scenarios, in terms of velocity, attitude and ground conditions. Below is shown the test matrix consisting of six landing configurations:

Configuration #	Vertical Velocity [m/s]	Horizontal Velocity [m/s]	Yaw [deg]	Pitch [deg]	Roll [deg]	Ground Condition
1	3.00	15	0	0	0	Dry
2	3.25	15	0	0	5	Dry
3	3.25	15	0	10	5	Dry
4	3.25	12	4	10	5	Dry
5	3.25	12	4	10	5	Wet
6	3.25	6	8	0	5	Dry

**Table 1** Test Matrix

Table 1 indicates that the attitude of the mock-up must be adjustable between tests with respect to yaw, roll, and pitch angles. In addition, the mock-up is required to achieve a minimum horizontal speed of 6 m/s and a maximum of 15 m/s, as well as a vertical speed in the range of 3 to 3.25 m/s. These specifications provided the basis for subsequent design and testing activities, ensuring that all experimental configurations could be accurately reproduced.

Moreover, to accurately reproduce the flight dynamics during the final landing phase, the representative mock-up of the Space Rider Re-entry Module is designed to meet the following geometric and mechanical requirements:

- For all six test configurations, the key requirements to be met concern Mass, Center of Gravity, and Inertia (MCI), which must remain within the prescribed tolerances with respect to the nominal RM values.
- Local static stiffness at the Landing Gear (LG) interfaces consistent with expected values, ensuring representative deformation under load.
- Fundamental frequency modes exceeding 31 Hz out-of-plane and 40 Hz in-plane, to prevent modal coupling.
- Capability to withstand environmental loads as well as the interface loads transmitted during landing.

Building on the definition of the main requirements, the following sections provide a detailed description of the design solutions adopted for the LTM and LTR, together with the corresponding verification activities.

## 3. Landing Test Rig

The LTM reaches the speed required by the test specification thanks to the Landing Test Rig (LTR), a railway structure 46 m long and 6 m high, equipped with an electrically propelled cart that carries the LTM. Fig. 1 shows a representation of the railway structure and cart vehicle, while Fig. 2 (Left) presents a CAD view of the LTM mounted on the cart.



Fig. 1 Railway Structure and Cart Vehicle in lower position

The cart is accelerated by four electric motors with rubber wheels preloaded on a beam, the motors are controlled by inverters, which regulate the cart speed. An additional advantage of the height of the structure is that it allows the use of smaller electric motors; without this height, larger and more expensive motors would be required to achieve the specified speed.

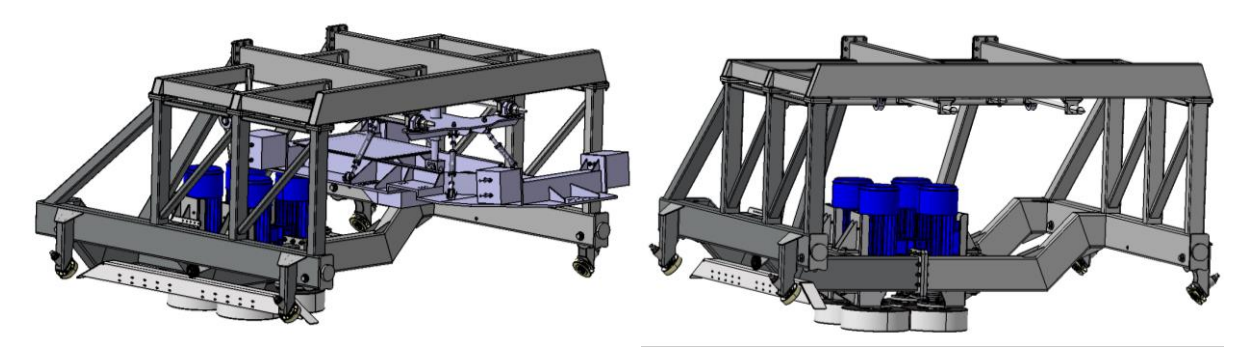


Fig. 2 Left: cart with LTM mounted. Right: cart without LTM.

The cart transports the LTM to a designated release point, where it detaches and begins falling freely. Separation is achieved passively using linear rails mounted on the cart and four ball bearing sleeves installed on the LTM, which remain engaged with the rails during transport. A mechanical stop prevents the LTM from sliding backward relative to the cart during acceleration. Upon the cart's contact with the bumpers, the sleeves slide along the rails to their ends, allowing the LTM to separate smoothly and initiate free fall.

The vertical velocity requirement can be achieved by releasing the LTM from a proper height. The maximum release height can be obtained as follows:

$$h_{release\_max} = \frac{{v_v}^2}{2g} = \frac{10.56}{19.62} = 0.54m$$
 (1)

Similarly, the resulting minimum release height is 0.46m. These release heights define the position of the lower part of the LTM (the first to touch the ground) according to the desired test conditions. Since the difference between the maximum and minimum release heights is about 0.08m, an adjustable structure (Fig. 3) has been designed. Positioned between the upper part of the cart and the linear guides, it consists of tubular sections that can be added or removed to accommodate the required height variations.

HiSST-2025-211 Page |3 Design of the Landing Stability Test for the ESA Space Rider Project

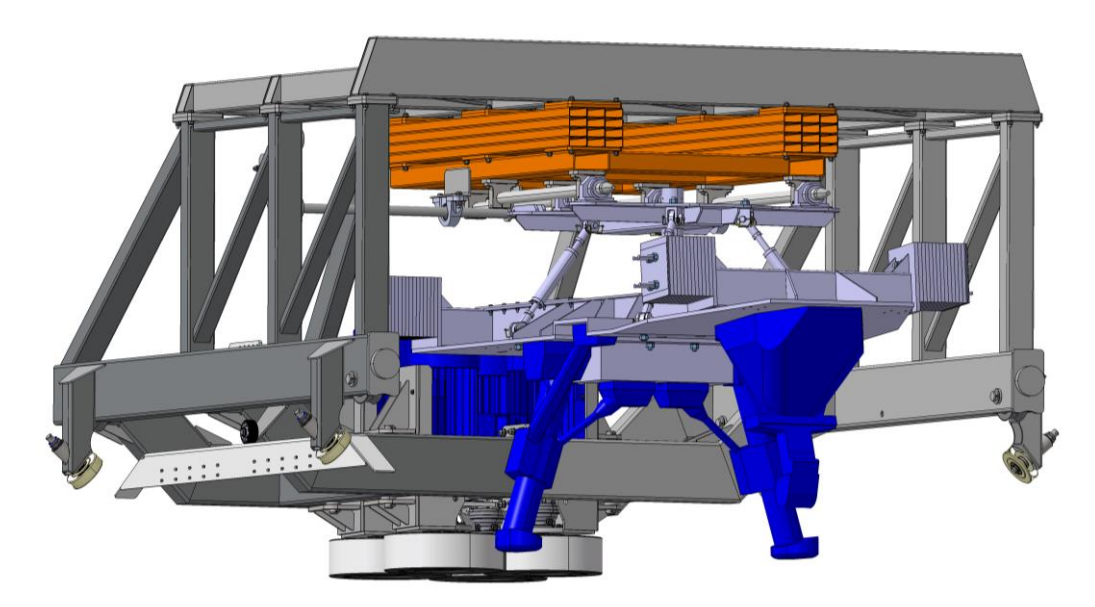


Fig. 3 Height-adjustment structure (orange) mounted between LTM and cart

# 4. Landing Test Model

The LTM consists of two primary elements: the Interface Assembly (IA), which connects the model to the LTR, and the Landing Assembly (LA), which reproduces the lower portion of the RM and houses the adjustable ballast system and the Landing Gear (LG). The LTM must replicate the mass distribution, inertial properties and structural behavior of RM as said in paragraph 2.

The various landing attitudes required for testing are achieved by rotating the LA relative to the IA through a universal joint that connects the two assemblies. After rotation, the LA is secured in position by four operating screws, which also facilitate the rotation. Each operating screw consists of two oppositely threaded tips connected by a hollow cylindrical element and is attached to the IA on one end and to the LA at the other via ball joint elements, allowing for smooth articulation during adjustment. Fig. 4 and Fig. 5 show the LTM CAD model.

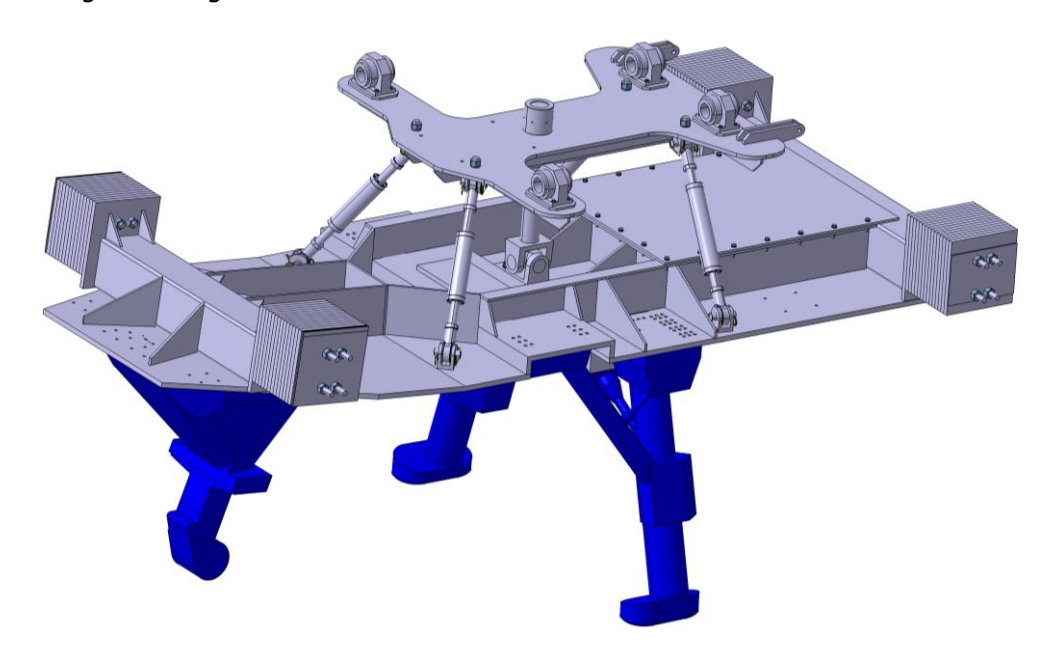


Fig. 4 Landing Test Model

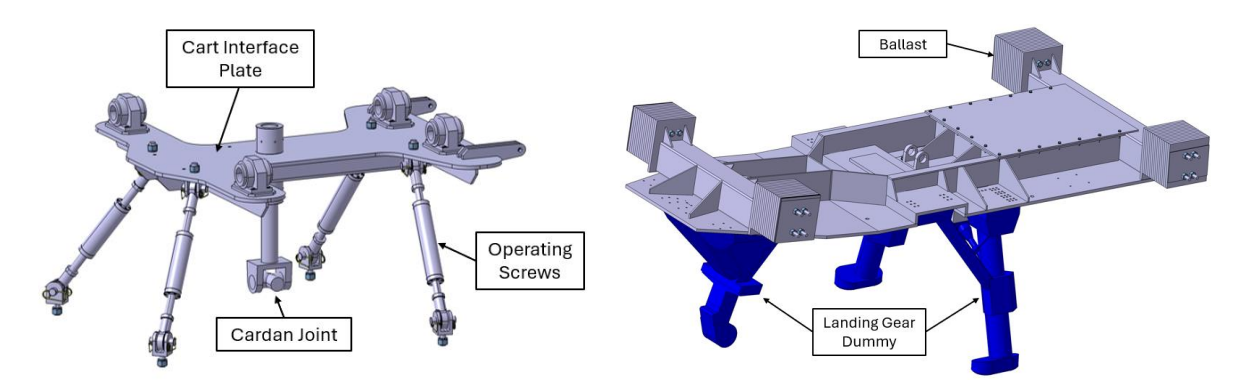


Fig. 5 Interface Assembly (left) and Landing Assembly (right)

To satisfy the MCI requirements, four ballasts are mounted to LA. Their weight and position are determined through an iterative process, as described in paragraph 5. The ballasts are made of steel and have a rectangular prism shape, with base dimensions of  $0.3~\text{m}\times0.3~\text{m}$  and a variable height depending on the required mass. Each ballast consists of multiple steel plates stacked together and secured by four threaded rods passing through the entire stack, with nuts at both ends.

Following the description of the LTM architecture, structural analyses were conducted to verify compliance with the prescribed stiffness and modal frequency requirements.

## 4.1. Local Stiffness Requirement Verification

To withstand the loads generated during ground impact, the LTM is designed to satisfy the local static stiffness requirements at the interface points with the Landing Gear (LG).

The stiffness assessment was carried out at each interface (Fig. 6) by applying a unit load separately along the x, y, and z directions, while constraining the remaining interface points.

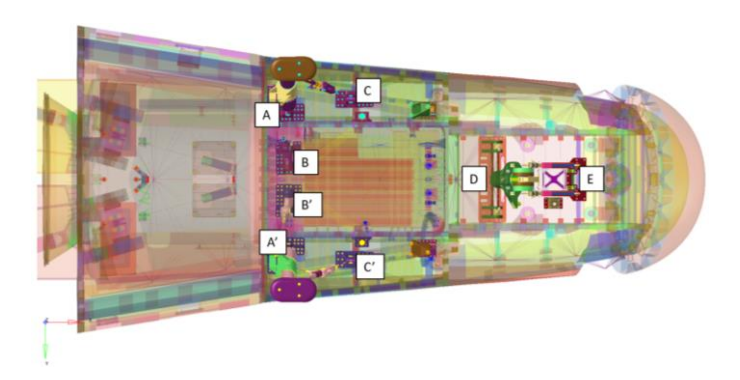


**Fig. 6** LTM-LG interface points

In the initial configuration, the interface areas B and B' did not comply with the prescribed stiffness values; consequently, the design was revised, as illustrated in Fig. 7.

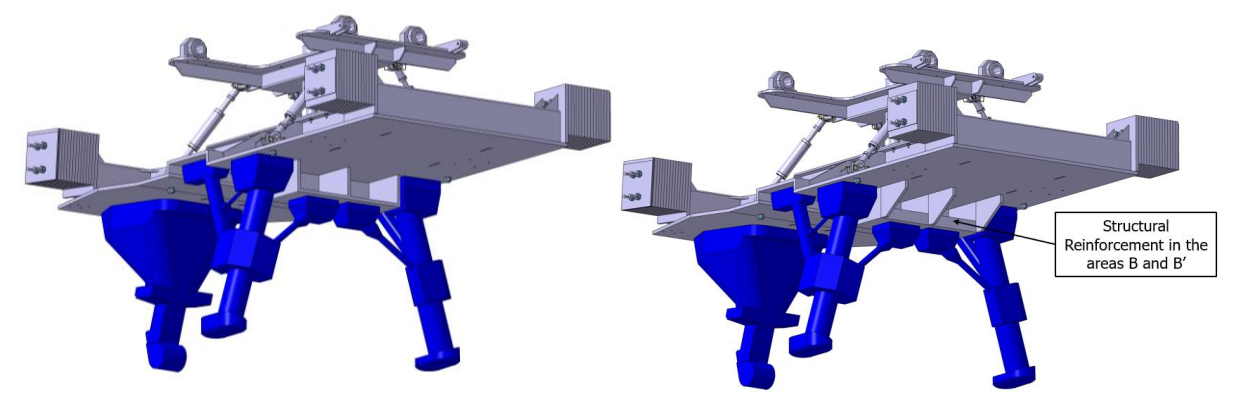


Fig. 7 Left: Initial design. Right: Reinforced design

The results of the updated analysis show that all stiffness requirements are now consistently met across the interface points. Table 2 shows the stiffness margins, calculated as:

$$Margin = \frac{Stiffness\ value}{Requirement} - 1$$

Table 2 Stiffness margins for each location and each direction at LTM-LG Interface points.

	LTM Stiffness margin				
Location	X dir.	Y dir.	Z dir.		
Α	1.70	7.79	0.31		
В	2.55	2.09	0.17		
С	1.32	24.37	0.27		
<b>A</b> ′	1.70	7.79	0.31		
B <sup>'</sup>	2.55	2.09	0.17		
<b>C</b> ′	1.32	24.37	0.27		
D	21.93	43.40	0.88		
E	10.83	37.52	0.37		

The verification of local stiffness at the LG interfaces confirmed the structural robustness of the LTM. Complementary to this analysis, modal simulations were performed to ensure that the fundamental frequency requirements were also satisfied, as described in the following section.

## 4.2. Minimum fundamental frequencies verification

The LTM is designed to satisfy the frequency requirements, with particular attention to the minimum fundamental modes in both out-of-plane (OOP) and in-plane (IP) directions. For the modal analysis, the LTM was constrained at the interface points to reproduce the actual boundary conditions during testing, as illustrated in Fig. 8. The operating screws and the central threaded rod were modeled as beam elements with circular cross-sections, while the ballasts were represented as concentrated masses connected to the supports via RBE2 elements.

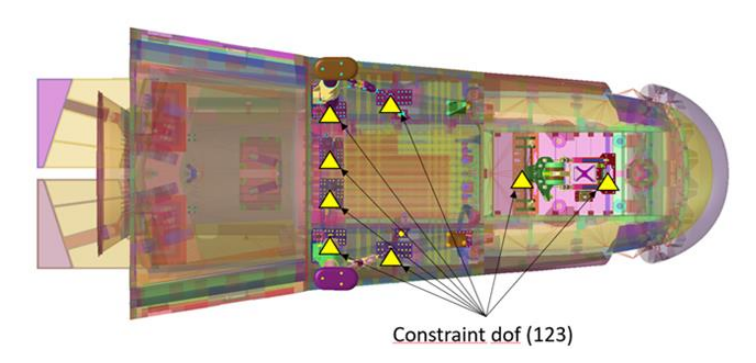


Fig. 8 Constraint points of the modal analysis

It is worth noting that the initial configuration did not include the cover plate shown in the Fig. 9; this component was later added to increase torsional stiffness, so that the torsional mode would occur at a sufficiently high frequency to meet the requirements.

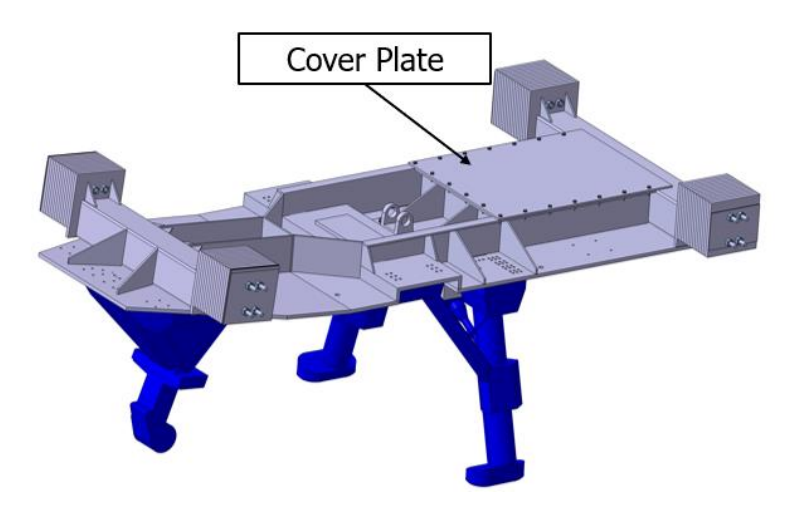


Fig. 9 Cover plate used to enhance torsional stiffness

The resulting fundamental frequencies margins are summarized in Table 3.

Table 3 LTM fundamental frequency results

Condition	Margin between calculated Frequency and requirement. [Hz]
1st 00P	11
1st IP	3

Fig. 10 and Fig. 11 show the behavior of the first vibration mode in-plane and out-of-plane, respectively.

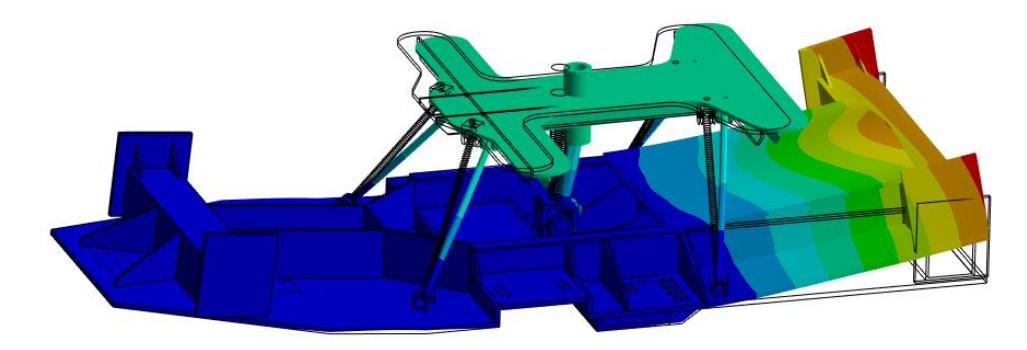


Fig. 10 1st OOP fundamental frequency

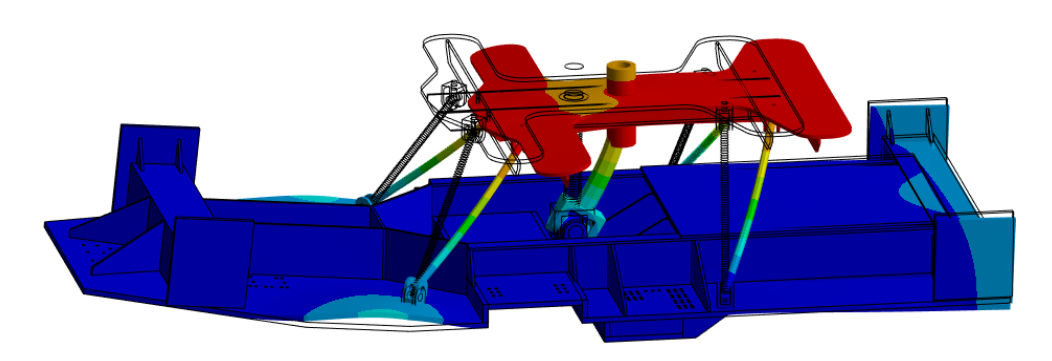


Fig. 11 1st IP fundamental frequency

Overall, the FEM analyses demonstrated that both stiffness and modal frequency requirements were satisfied, providing a reliable structural baseline for the subsequent optimization of the ballast system and verification of the LTM inertial properties.

Page |7

## 4.3. Environmental requirements verification

Finally, to assess the LTM's structural capability to withstand the interface loads transmitted by the landing gear, a set of finite element analyses was carried out considering the different load cases experienced by the Space Rider RM during landing.

The landing loads were applied to the master node (located at the outermost point of the landing gear) of the RBE2 elements connected to the landing gear brackets, as shown in Fig. 12, while the operating screws and the ballasts were modeled as described in the paragraph of frequencies verification.

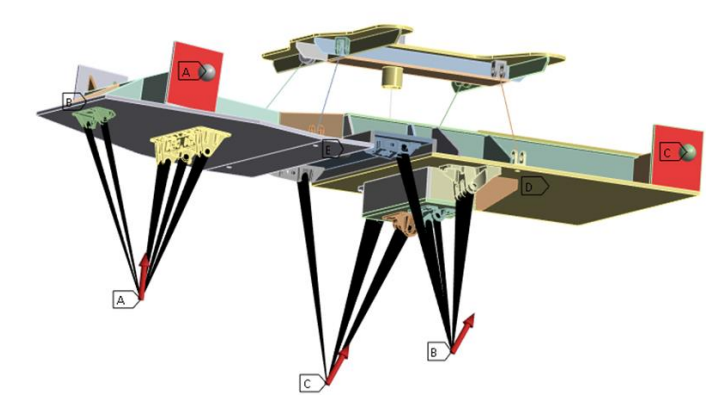


Fig. 12 LTM finite element model with applied interface load

Figures below show the LTM model with the applied loads and the corresponding stress distribution from one of the most critical landing load cases.

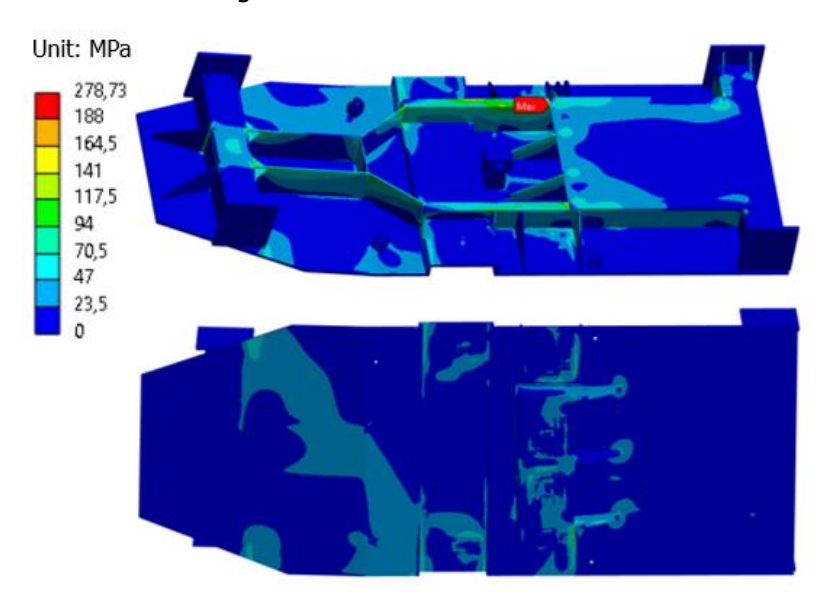


Fig. 13 Von Mises Stress Results of LA

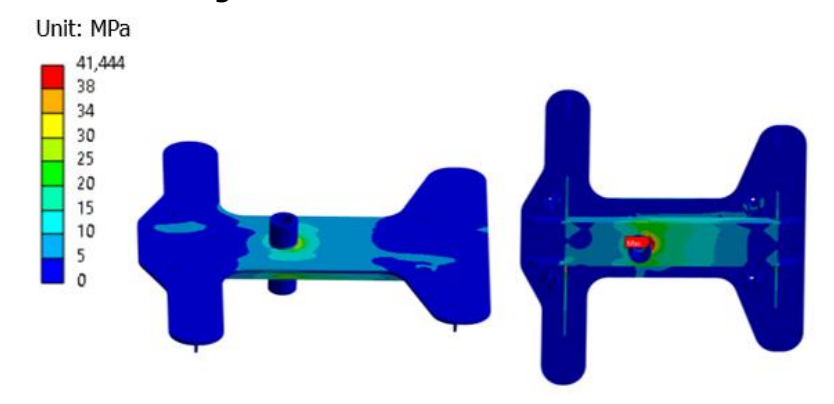


Fig. 14 Von Mises Stress Results of IA

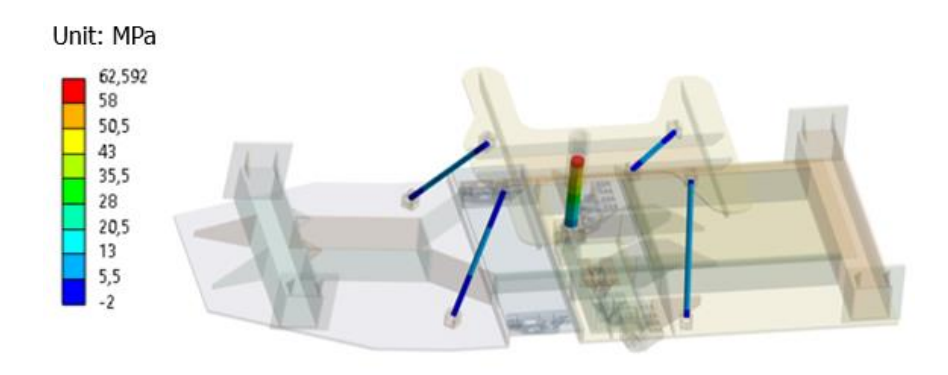


Fig. 15 Maximum Combined Stress results of operating screws

The results shown in the figures confirm the robustness of the steel test article, with maximum stress remaining within manageable and acceptable levels.

## 5. Iterative Design Process

The design process, including ballasts definition and verification of Mass, Center of gravity, and Inertia (MCI) properties, is carried out through an iterative multi-variable optimization. This approach is necessary because any change in geometry (for example to satisfy stiffness and modal frequency requirements) affects the mock-up's mass, CoG, and inertia. Moreover, since the mock-up has a rotatable section to vary its attitude, the MCI requirements change with orientation (Fig. 16). The iterative optimization identifies a single ballast configuration that meets all requirements across six test setups.

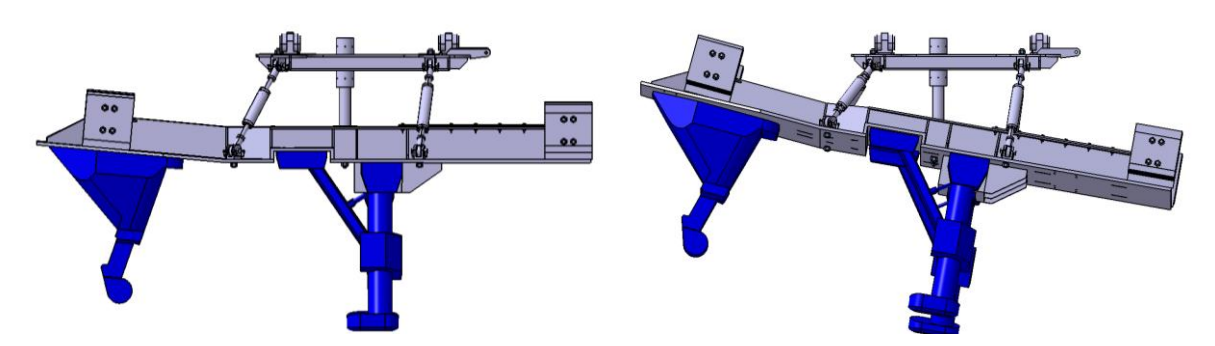


Fig. 16 Configuration #1 and #3 of LTM

The optimization variables are the N ballast masses and the 3N components of their centers of gravity, forming the input vector:

$$\underline{r} = [m_1, \dots, m_N, x_1, y_1, z_1, \dots, x_N, y_N, z_N]^T$$
(2)

This vector serves as input to the scalar objective function J(r), which quantifies deviations from the target mass, CoG, and inertia:

$$J(\underline{r}) = |\delta_M|^2 + \|\delta_{COG}\|^2 + \|\delta_I\|^2 + P(\underline{r})$$
(3)

 $\delta_{\rm M}$  is the scalar deviation of the LTM mass normalized by the respective tolerance:

$$\delta_M = \frac{M_{req} - M_{LTM}(\underline{r})}{2 \ tol_M} \tag{4}$$

whilst  $\delta_{CoG}$  and  $\delta_I$  are the vectors whose components are the deviations of the relative CoG and inertias components, normalized by their respective tolerance:

$$(\delta_{CoG})_i = \frac{\left(CoG_{req}\right)_i - \left(CoG_{LTM}(\underline{r})\right)_i}{2\left(tol_{CoG}\right)_i} \quad i = 1,2,3$$
 (5)

HiSST-2025-211 Design of the Landing Stability Test for the ESA Space Rider Project

$$(\delta_l)_j = \frac{\left(I_{req}\right)_j - \left(I_{LTM}(\underline{r})\right)_j}{2\left(tol_l\right)_j} \quad j = 1, \dots, 6$$
(6)

The penalty function,  $P(\underline{r})$ , ensures solutions remain within prescribed tolerances:

$$P(\underline{r}) = \alpha_M * p(\delta_M) + \alpha_{COG} * \sum_{i=1}^{3} p((\delta_{COG})_i) + \alpha_I * \sum_{j=1}^{6} p((\delta_I)_j)$$
 (7)

$$p(x) = \begin{cases} |x| & if \ |x| > 1\\ 0 & otherwise \end{cases}$$
 (8)

Weighting coefficients  $\alpha_{CoG}$ ,  $\alpha_{M}$  and  $\alpha_{I}$  balance the contributions of mass, CoG, and inertia. The objective function is minimized using MATLAB's fmincon, with boundary conditions varying at each step. A flow chart of the ballast definition routine is presented in Fig. 17.

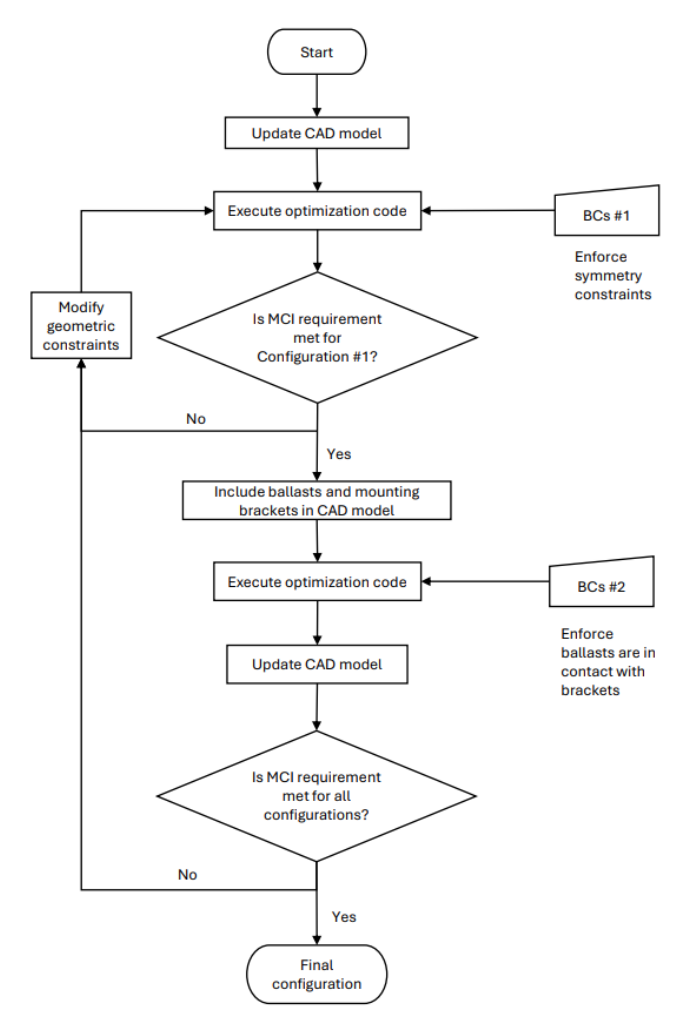


Fig. 17 Flow chart of ballasts' definition routine

The first set of boundary conditions (Eq. 9) enforce the symmetry of ballasts positions with respect to the LTM symmetry plane and is applied early in the optimization routine to obtain an initial symmetric configuration. No constraint was imposed on individual ballast masses, allowing controlled asymmetry to satisfy the non-zero products of inertia:

$$\begin{cases} x_{2i-1} = x_{2i} \\ y_{2i-1} = -y_{2i} & i = 1, ..., N/2 \\ z_{2i-1} = z_{2i} \end{cases}$$
 (9)

In a later stage, a second set of boundary conditions (Eq. 10) ensures that, although each ballast could be asymmetric in mass, it remained in contact with its respective mounting bracket, while the remaining components of the position vector were kept at previously determined values:

HiSST-2025-211 Page |10 Copyright © 2025 by authors

$$\begin{cases} y_{2j-1} = \frac{x_i = x_{0i}}{m_{2j-1} - m_{2j}} - y_{2j} & i = 1, ..., N \quad j = 1, ..., N/2 \\ z_i = z_{0i} & \end{cases}$$
 (10)

The number of ballasts N and two of their dimensions is selected by the designer. For simplicity and to facilitate manufacturing, four steel ballasts were initially assumed, with rectangular prism shapes and base dimensions  $a = 0.3 \, m$   $b = 0.3 \, m$ . The third dimension is determined based on the target mass, assuming a steel density of  $\rho = 7860 \ kg/m^3$ .

Additional inequality constraints were implemented to account for geometric limitations. For N=4, these constraints were:

$$\begin{cases} 0 \leq m_{i} \leq m_{max} [kg] \ i = 1, ..., N \\ x_{min,1} \leq {x_{1} \choose x_{2}} \leq x_{max,1} [m] \\ x_{min,3} \leq {x_{3} \choose x_{4}} \leq x_{max,3} [m] \end{cases}$$

$$\begin{cases} y_{min,1} \leq {y_{1} \choose -y_{2}} \leq y_{max,1} [m] \\ y_{min,3} \leq {y_{3} \choose -y_{4}} \leq y_{max,4} [m] \end{cases} \begin{cases} z_{min,1} \leq {z_{1} \choose z_{2}} \leq z_{max,1} [m] \\ z_{min,3} \leq {z_{3} \choose -y_{4}} \leq y_{max,4} [m] \end{cases}$$

$$(11)$$

$$\begin{cases} y_{min,1} \le {y_1 \choose -y_2} \le y_{max,1} [m] & z_{min,1} \le {z_1 \choose z_2} \le z_{max,1} [m] \\ y_{min,3} \le {y_3 \choose -y_4} \le y_{max,4} [m] & z_{min,3} \le {z_3 \choose z_4} \le z_{max,4} [m] \end{cases}$$
(12)

Table 4 and Table 5 compare the MCI tolerances required by the test specifications for the LTM without landing gear, and the values obtained from the LTM CAD model for each landing configuration. Only five conditions are shown, as configurations #5 and #6 differ solely in the terrain condition.

Table 4 Comparison between required and obtained tolerances for Mass and Cog position for each designed LTM configuration

	Mass	XcoG	YcoG	Z <sub>CoG</sub>
	[kg]	[mm]	[mm]	[mm]
Required Tolerance	±33	±11	±5	±8
N# Configuration				
1	11.2	1	0	0
2	11.2	1	4	-6
3	11.2	10	4	-4
4	11.2	10	3	-4
5	11.2	1	3	-6

**Table 5** Comparison between required and obtained tolerances for moment of inertia data of each designed LTM configuration

	J <sub>XX</sub>	$\mathbf{J}_{\mathbf{YY}}$	Jzz	J <sub>XY</sub>	J <sub>XZ</sub>	$\mathbf{J}_{YZ}$
	[kg m²]	[kg m²]	[kg m²]	[kg m²]	[kg m²]	[kg m²]
<b>Required Tolerance</b>	±197	±902	±937	±30.0	±58.6	±10.0
N# Configuration						
1	3.2	-354	116	0.5	0.2	-0.6
2	-7.8	-365	116	-16.7	23.4	-2.3
3	-3.4	-291	186	-17.1	17.9	-2.5
4	-3.3	-290	186	-15.2	17.6	-1.4
5	-7.3	-364	117	-13.1	23.0	-0.6

## 5.1.CoG experimental verification

The CoG position of the LTM in the XY plane will be experimentally determined using three jacking points, each equipped with a load cell. These points, labeled A, B, and C, are shown in the Fig. 18; the supports connected to the jacking points are highlighted in red.

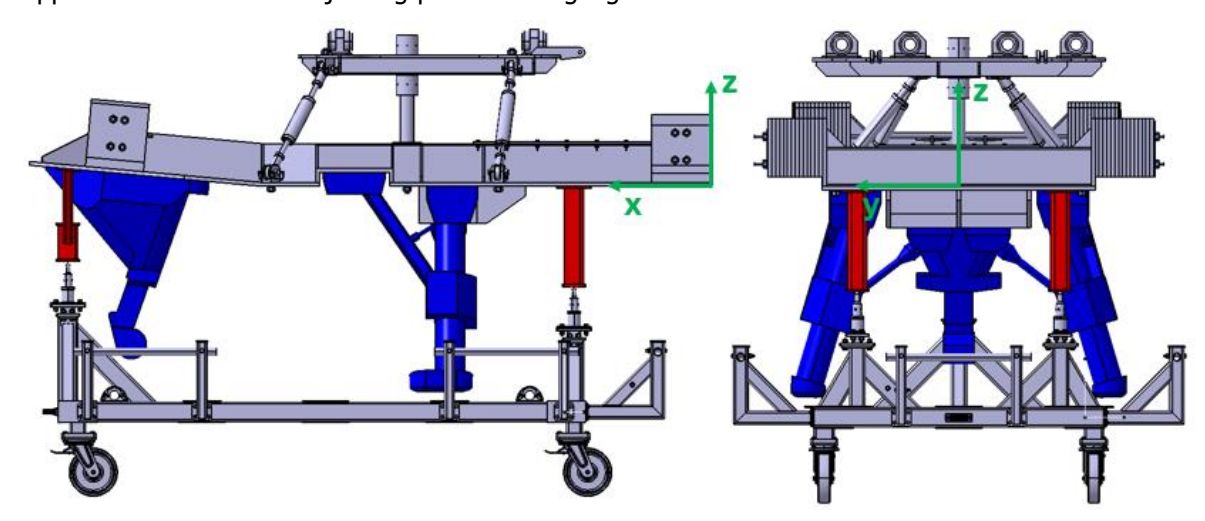


Fig. 18 LTM engaged on the MGSE-Trolley via Jacking points

By measuring the reaction forces at the three locations and exploiting the known geometry of the jacking points, both the total mass of the LTM and the CoG coordinates in the XY plane can be computed. The calculation is based on the classical vector relation for the center of gravity of a system of concentrated masses (Eq. 13) where  $\overrightarrow{r_{cog}}$  and  $\overrightarrow{r_i}$  are the position vectors of the CoG and of points A, B and C, respectively:

$$\vec{r}_{COG} = \frac{\sum_{i=A}^{C} \vec{r}_{i} W_{i}}{\sum_{i=A}^{C} W_{i}}$$
 (13)

The total weight of the LTM is simply given by the sum of the three load cells reading (Eq. 14):

$$W_T = \sum_{i=A}^{C} W_i = W_A + W_B + W_C \tag{14}$$

From the component-wise development, the CoG coordinates are obtained as (Eq. 15 - Eq.16):

$$x_{COG} = \frac{x_A W_A + x_B W_B + x_C W_C}{W_A + W_B + W_C} \tag{15}$$

$$y_{COG} = \frac{y_A W_A + y_B W_B + y_C W_C}{W_A + W_B + W_C}$$
 (16)

### 6. Conclusions

The Landing Stability Test system for the Space Rider Re-entry Module has been designed in full compliance with the program requirements, as verified through detailed structural and modal analyses. The iterative design methodology, combining FEM analyses, ballast optimization, and tailored mock-up development, has proven effective and can serve as a valuable reference for similar dynamic test campaigns.

Future work will focus on the realization of the hardware components required for testing, the experimental determination of the center of gravity, and the execution of the full-scale Landing Stability Test at CIRA where the dedicated facility is currently under development. These next steps will provide the final validation of the system and further consolidate the methodology as a tool for designing and qualifying complex landing subsystems.

HiSST-2025-211 Page |12 Copyright © 2025 by authors

## 7. Acknowledgment

The authors would like to thank Thales Alenia Space Italia (TAS-I) for its Prime Contractor role and for the technical support provided, indeed the Landing Stability Test activity is the result of a close cooperation between technicians from CIRA and TAS-I. Authors acknowledge the European Space Agency (ESA), leader of the Space Rider Program, the Italian Space Agency, Avio, Incas and all the partners involved in the Space Rider program for their continuous support and collaboration.

Special thank go to the Italian company Extreme Engineering that supported CIRA in transferring their roller coaster expertise and technology into our special test necessity. Their expertise and contributions have been fundamental to the development and success of this work.

#### References

- [1] Oprea, Burlou, Guidotti, Vernillo, Rufolo, Pisano, Cuciniello, and others: "Mission Analysis and Feasibility Assessment for the System Drop Test of ESA Space Rider Re-Entry Module" 75th International Astronautical Congress (IAC 2024)
- [2] Garbarino, Morani, Vernillo, Cuciniello, Battipede, Mallardo, Rufolo: "Real-Time Hardware-in-theloop Test-Rig for Space Rider'S Drop Test" AIAA 2025-3727
- [3] Vernillo, Rufolo, Cuciniello, Pisano, De Fenza, Brinza, Popa, Mareschi, Sudars: "SPACE RIDER: DESIGN OF A SYSTEM DROP TEST FOR THE VALIDATION OF THE DESCENT AND LANDING MISSION PHASE". FAR 19-23 June 2022.
- [4] Vernillo, Rufolo, De Fenza, Cuciniello, Pisano, Fauci, Mareschi, Brinza, Marin, Ascanio: "SDT, UPDATES OF THE DESIGN OF A SYSTEM DROP TEST FOR THE VALIDATION OF THE DESCENT AND LANDING PHASE OF THE SPACECRAFT". FAR 18-22 May 2025.